

Proton emission from cone-in-shell fast-ignition experiments at Omega

N. Sinenian, W. Theobald, J. A. Frenje, C. Stoeckl, F. H. Séguin et al.

Citation: *Phys. Plasmas* **19**, 112708 (2012); doi: 10.1063/1.4767636

View online: <http://dx.doi.org/10.1063/1.4767636>

View Table of Contents: <http://pop.aip.org/resource/1/PHPAEN/v19/i11>

Published by the [American Institute of Physics](#).

Related Articles

K-shell spectroscopy of silicon ions as diagnostic for high electric fields
Rev. Sci. Instrum. **83**, 113507 (2012)

Landau damping effects on the scattering spin-asymmetry and channel preference in election-hole plasmas
Phys. Plasmas **19**, 112112 (2012)

Charged electret deposition for the manipulation of high power microwave flashover delay times
Phys. Plasmas **19**, 112111 (2012)

The simplest equivalent circuit of a pulsed dielectric barrier discharge and the determination of the gas gap charge transfer
Rev. Sci. Instrum. **83**, 115112 (2012)

Influence of lateral target size on hot electron production and electromagnetic pulse emission from laser-irradiated metallic targets
Phys. Plasmas **19**, 113116 (2012)

Additional information on *Phys. Plasmas*

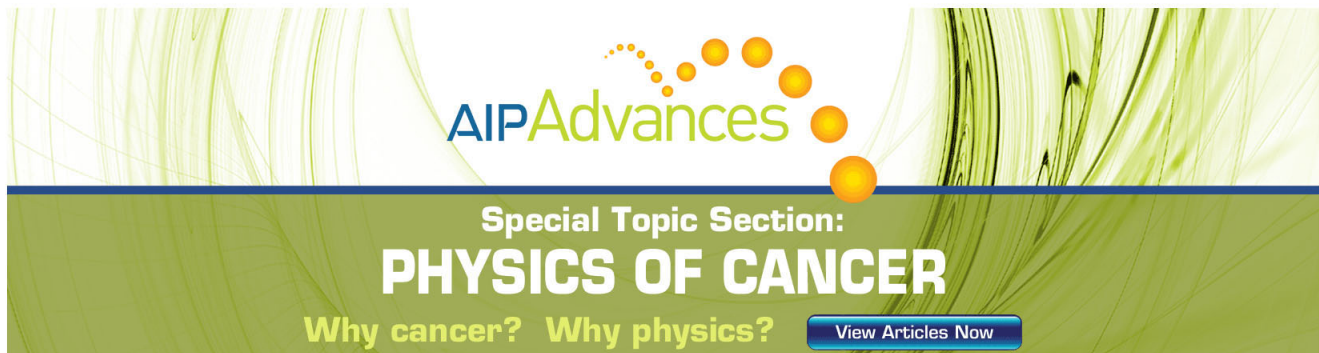
Journal Homepage: <http://pop.aip.org/>

Journal Information: http://pop.aip.org/about/about_the_journal

Top downloads: http://pop.aip.org/features/most_downloaded

Information for Authors: <http://pop.aip.org/authors>

ADVERTISEMENT



AIP Advances

Special Topic Section:
PHYSICS OF CANCER

Why cancer? Why physics? [View Articles Now](#)

Proton emission from cone-in-shell fast-ignition experiments at Omega

N. Sinenian,^{1,a)} W. Theobald,² J. A. Frenje,¹ C. Stoeckl,² F. H. Séguin,¹ C. K. Li,¹
 R. D. Petrasso,¹ and R. B. Stephens³

¹Plasma Science and Fusion Center, Massachusetts Institute of Technology, Cambridge, Massachusetts 02139, USA

²Laboratory for Laser Energetics, Rochester, New York 14623, USA

³General Atomics, San Diego, California 92186, USA

(Received 4 June 2012; accepted 31 October 2012; published online 28 November 2012)

Measurements of energetic protons from cone-in-shell fast-ignition implosions at Omega have been conducted. In these experiments, charged-particle spectrometers were used to measure a significant population ($>10^{13}$) of energetic protons (7.5 MeV max.), indicating the presence of strong electric fields. These energetic protons, observed in directions both transverse and forward relative to the direction of the short-pulse laser beam, have been used to study aspects of coupling efficiency of the petawatt fast-ignitor beam. Approximately 5% of the laser energy coupled to hot electrons was lost to fast ions. Forward going protons were less energetic and showed no dependence on laser intensity or whether the cone tip was intact when the short-pulse laser was fired. Maximum energies of protons emitted transverse to the cone-in-shell target scale with incident on-target laser intensity ($2\text{--}6 \times 10^{18} \text{ W-cm}^{-2}$), as described by the ponderomotive scaling ($\propto I^{1/2}$). It is shown that these protons are accelerated from the entire cone, rather than from the cone tip alone. These protons were used to estimate the lower limit on the hot-electron temperature, which was found to be hotter than the ponderomotive scaling by factors of 2–3. © 2012 American Institute of Physics. [<http://dx.doi.org/10.1063/1.4767636>]

I. INTRODUCTION

The fast-ignition concept^{1,2} has been described thoroughly in the literature as one alternative to direct-drive hot-spot ignition. In this scheme, a high-energy, high-intensity ($10^{15} \text{ W-cm}^{-2}$) laser is used to compress a cold shell containing fusion fuel to high areal densities ($\rho R \sim 1 \text{ g-cm}^{-2}$). A short-pulse, ultrahigh-intensity laser ($10^{19} \text{ W-cm}^{-2}$) is then used to generate megavolt electrons to heat the core of the compressed fuel in a time short compared to hydrodynamic timescales. The use of two independent laser drivers for compression of the fuel and subsequent heating of the core allows for higher target gains, in principle, for the same amount of driver energy. This is because high fuel areal-density cores can be assembled with slow implosion velocities and ignition is achieved through efficient coupling of short-pulse beam energy to the dense core.¹ In comparison to conventional hot-spot ignition, the symmetry requirement of the fuel assembly in fast ignition is not as stringent, which relaxes the illumination uniformity and power balance constraints of the driver.

The success of this approach relies on the effective energy coupling between the short-pulse laser and the compressed fuel. A high coupling efficiency (CE) depends on the generation of hot electrons and their transport and energy deposition to the dense fuel core. A potential problem is that the generation of energetic electrons will inevitably accelerate ions as well. Any energy coupling to ions is a direct loss channel that must be examined.

The acceleration of ions by electrostatic sheath fields generated by laser-plasma-interaction (LPI) produced hot

electrons has been observed in both direct-drive³ and indirect-drive⁴ configurations with $\sim 10^{14} \text{ W-cm}^{-2}$ long-pulse beams. Protons and heavier ions produced by ultra-intense ($\sim 10^{18}\text{--}10^{19} \text{ W-cm}^{-2}$) short-pulse LPI have also been studied extensively using flat foil and cone targets. In short-pulse scenarios, laser-to-proton energy conversion efficiency, angular emission of protons from flat-foil targets, focused emission of proton beams, and effects of plasma scale length on proton acceleration have been studied.^{5–7} Proton measurements have also been used, in conjunction with ion expansion models,^{8–10} to infer the temperature of the LPI-generated hot-electron distribution that accelerates these protons.^{11,12}

In this paper, we present the first measurements of fast protons from cone-in-shell fast-ignition implosions conducted at the Omega Laser Facility.^{13,14} In these experiments, a short-pulse laser was focused into gold cones to generate hot electrons that subsequently heat a pre-assembled dense D_2 core, with the aim to increase the DD-neutron yield by raising the ion temperature.¹⁵ For these experiments, the neutron yield enhancement due to core heating has been measured previously to be a factor of ~ 4 , corresponding to a CE of 3.5%.¹⁵

In the context of proton acceleration, these experiments differ from the previous work with cone-in-shell targets and short-pulse lasers in that (1) protons have been used here as a diagnostic tool to assess effectiveness of fast-ignitor coupling to the dense core and (2) to determine the energy coupling to protons, an energy loss mechanism in fast-ignition experiments.

This paper is organized as follows: Sec. II presents an overview of the experimental setup and charged-particle

^{a)}nareg@psfc.mit.edu.

diagnostics used to measure proton spectra. In Sec. III, proton spectra and maximum energies are presented, followed by a discussion in Sec. IV of where the protons are accelerated from. In Sec. V, protons are used to estimate the hot-electron temperature for these experiments. Sec. VI concludes by summarizing the results of this paper.

II. EXPERIMENTS

The experiments were performed at the Omega Laser Facility located at the Laboratory for Laser Energetics, University of Rochester. Both the OMEGA (long pulse) and OMEGA EP (short pulse) lasers were used. OMEGA is a 60 beam neodymium-glass laser capable of focusing 30 kJ of frequency-tripled light at a wavelength of 351 nm to on-target intensities greater than 10^{15} W-cm⁻². OMEGA EP consists of four beams. Two of these beams are short pulse, each capable of delivering 1 kJ of 1053 nm light in 10 ps, while the other two are long pulse. In these experiments,¹⁵ 54 OMEGA beams delivering 18 kJ of UV light to the capsule were used to compress the target along a low adiabat ($\alpha \approx 1.5$), which was achieved using a short single picket, followed by a main drive pulse with a duration of approximately 2.7 ns. A single short-pulse (~ 10 ps) Gaussian-shaped OMEGA EP beam was then brought to focus inside the OMEGA target chamber. At best focus, 80% of the beam energy was contained within a diameter of approximately 50 μ m, resulting in a maximum, beam-averaged on-target intensity of $\approx 6 \times 10^{18}$ W-cm⁻². For these experiments, the OMEGA EP power and energy contrast were of order 10^6 and 10^4 , respectively.¹⁵ Details on the targets can be found in Ref. 15. In summary, the targets for these experiments were re-entrant gold cones inside 40- μ m-thick deuterated-plastic (CD) shells with a nominal diameter of 870 μ m. The cones were either 1.2 or 1.8 mm in length and had an opening half-angle of 17°. The cone tips were flat with variable tip thickness (5–15 μ m) and tip diameter of 10 μ m. The cone walls were 10- μ m-thick inside the shell and 50- μ m-thick outside. The shells were not gas-filled, leaving only the CD shell and the ablated material from it to undergo fusion.

Proton energy spectra were measured using both the magnet-based charged-particle spectrometer (CPS1) and wedge-range-filter (WRF) spectrometers.¹⁶ These instruments utilize CR-39 solid-state nuclear track detectors (SSNTD), which are known to provide information about the energy and species of the detected charged-particles.¹⁶ It has been shown recently, however, that there exists CR-39 piece-to-piece variability in its response to charged-particles.¹⁷ Thus, CR-39 alone cannot be used for accurate measurements of charged-particle spectra and must be paired with an additional particle dispersion mechanism. CR-39 is immune to electromagnetic pulse (EMP) and to some extent to x-rays, making it ideal for short-pulse experiments such as those presented here.

CPS1 features a 0.1-mm slit and a 7.6-kG magnet for dispersion of charged-particles onto CR-39 detectors. These spectrometers are capable of measuring proton energy spectra in the range of 200 keV to 30 MeV. The low energy limit is set by filtering (directly in front of the CR-39), which is required to mitigate a very large flux of low-energy charged-particles

that would otherwise scatter within the diagnostic and saturate the detector. The high energy limit is set by the magnet dispersion and detector arrangement. CPS1 is fixed to the OMEGA target chamber as shown in Fig. 1. In practice, the exponential energy spectra of short-pulse accelerated protons results in a large on-detector proton fluence at lower energies. This may cause saturation of the CR-39 detector at these energies, effectively raising the low-energy limit of this diagnostic. It is worth noting that CPS1 cannot resolve heavy ions because of the degeneracy between charge state, mass, and energy that exists for magnetic spectrometers.¹⁶ Filters constructed of mylar and aluminum are overlaid on the CR-39 to filter out these ions. Furthermore, any energetic heavy ions that penetrate the filters are separated from protons on the basis of the contrast and diameter of the tracks they leave on the CR-39.

The WRF spectrometers use CR-39 overlaid with a piece of wedge-shaped zirconia ceramic (ZrO₂), in which the minimum particle energy required to penetrate the wedge varies along the thickness (dispersion) direction. Since the zirconia wedge cannot be made thinner than 40 μ m, the low-energy instrument cutoff for measurement of protons is approximately 3–4 MeV. The WRFs are compact (5 cm across) spectrometers that are ideal in probing the implosion at several locations. Several (either 3 or 5) WRF modules, each consisting of two WRFs, were used at a single measurement location to obtain good statistics. Fig. 1 shows the azimuthal projection of the location of these spectrometers in the OMEGA target chamber relative to the short-pulse beam and target. The coordinate system is defined such that the pole (0°) corresponds to the direction of the short-pulse laser.

The WRF proton spectrometers were the primary diagnostics. These were fielded on nearly every shot, while CPS1 was fielded on a handful of shots to corroborate the WRF measurements and provide additional details of the spectrum at energies below the WRF low-energy cutoff. The spectrometers subtend small solid angles (1 μ sr for CPS1 and 100 μ sr for the WRFs). They measured protons accelerated normal to the CD shell surface for the locations shown in Fig. 1. In addition, when fielded at 80°, the spectrometers measured protons accelerated nearly normal to the cone

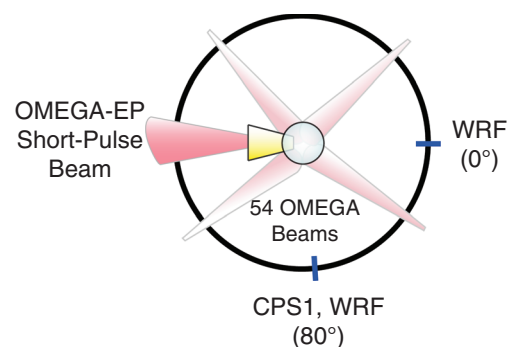


FIG. 1. Schematic of the experimental setup. The charged-particle spectrometers CPS1 and WRFs, positioned at different azimuthal angles, were used in these experiments. The coordinate system is defined such that the pole (0°) corresponds to the direction of the short-pulse laser. The OMEGA beams were used to first compress the CD shell, after which the short-pulse EP beam was used to produce energetic electrons to heat the deuterium fuel.

surface since that surface is nearly parallel to the spectrometer aperture due to the 17° cone opening half-angle.

III. PROTON SPECTRA AND MAXIMUM ENERGIES

A typical proton energy spectrum from integrated experiments, acquired using CPS1 (OMEGA Shot 56971) is shown in Fig. 2. Alongside this spectrum is the proton spectrum for a reference implosion (OMEGA Shot 56976), where a similar target was imploded using the same long-pulse configuration (~ 20 kJ, 54 OMEGA beams) without any short-pulse core heating. It is well established that long-pulse LPI generate protons up to about ~ 1 MeV,^{3,18} consistent with the data shown for the reference implosion. Nearly all of the observed energetic protons, however, arise from short-pulse LPI. These spectra exhibit a high-energy cutoff corresponding to the maximum path-integrated electric fields seen by the ions.

Proton energy spectra were measured down to approximately 200 keV using the CPS. As proton emission was anisotropic, it was difficult to measure the total energy lost to protons with precision. On the basis of measurements such as the one shown in Fig. 2, we estimate that the total energy carried by these protons is about 10 J, or about 1% of the incident short-pulse laser energy. This number can be compared to the previously inferred 20% coupling efficiency of short-pulse laser energy to hot electrons.¹⁹ In other words, approximately 5% of the short-pulse laser energy coupled to hot electrons is lost to the acceleration of ions.

The fact that the observed ions were protons (and not deuterons or heavier ions) was confirmed by simultaneous charged-particle measurements using CPS1 and WRF spectrometers. Since CPS1 uses magnetic fields for ion dispersion, it can be shown that the inferred energy of an ion depends inversely on the assumed ion mass.¹⁶ Thus, the CPS1-inferred energy of a deuteron mistakenly identified as a proton will be twice as large as the actual particle's energy. The WRFs have an opposite energy-mass dependence, whereby the inferred energy of a deuteron mistakenly identified as a proton will be lower than the actual particle's

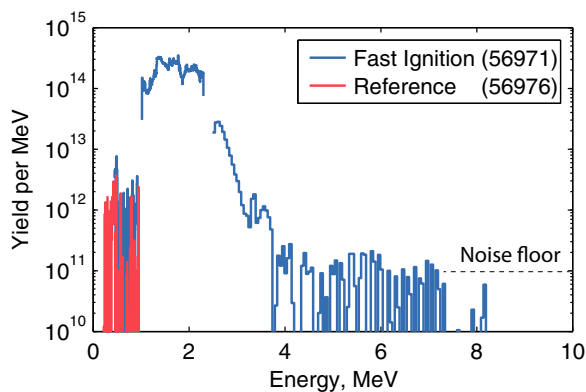


FIG. 2. Proton spectra measured with CPS1 (80°) on a fast-ignition shot and reference shot. In both cases, a gold cone-in-shell target was compressed using 54 OMEGA beams (~ 20 kJ) and a low-adiabat laser drive. For the fast-ignition case, an EP short-pulse laser was fired, at peak compression of the target, to generate hot electrons and heat the dense core. These energy spectra were background subtracted, although some residual background is observed in the 4–7 MeV range. The gaps in spectrum at ~ 1 MeV and ~ 2.3 MeV are due to the instrument.

energy. Thus, it is possible to constrain the particle species using these measurement techniques on the same shot and same polar angle. In particular, CPS1 and the WRFs measure particles at the same polar angle (80°) but different azimuthal angles.

Since the target is composed of a CD shell and Au cone, these protons originate predominantly from hydrocarbon contaminants on the surface of the target (either from the cone or shell) that may or may not have been blown off during the implosion of the shell. In any case, the implications are that the protons do not significantly interact or scatter with the compressed shell. The cone-in-shell target conditions at the time when the short-pulse laser interacts with the cone are schematically illustrated in Fig. 3. Shown are the cone, the compressed D_2 core (~ 50 - μm diameter), the blow-off plasma surrounding the target, the generated hot electrons and the accelerated protons. The relative timing between the short-pulse laser and the start of the long-pulse compression lasers was varied from shot-to-shot, but was typically 3 ns. At this point in time, the blowoff plasma from the ablated shell has expanded with the ion sound speed ($c_s \equiv \sqrt{T/m_i}$), resulting in a characteristic scale length of about 400 μm –1 mm for typical coronal temperatures of ~ 2 keV. The blowoff plasma from the implosion of the shell thus surrounds the target, and it is expected that the fast-protons are accelerated in the presence of this long-scale-length plasma.

The maximum proton energy is of interest since it scales directly with the temperature of short-pulse-generated hot electrons.^{20,21} Direct measurements of the maximum energy can therefore be used to qualitatively infer how the hot-electron temperature varies with experimental parameters. The maximum proton energy was measured at various locations around the implosion using the compact WRF spectrometers on several shots (Fig. 4). These data incorporate gold cones with 5- μm , 10- μm and 15- μm -thick tips and 10- μm tip diameters. The data obtained in the direction transverse to the short-pulse beam (80°) scale with intensity. A χ^2 -analysis indicate that these data fit a normalized ponderomotive scaling ($\propto I^{1/2}$) at 80° (reduced $\chi^2 = 0.96$). This further confirms that these protons are accelerated by short-pulse generated hot electrons. Since the maximum energies

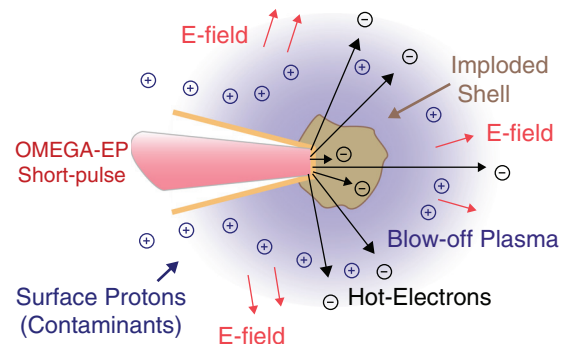


FIG. 3. Schematic of the target conditions when the short-pulse OMEGA EP laser interacts with the cone tip. The CD shell has been compressed to a diameter of ~ 50 μm , and is surrounded by blowoff plasma from the ablated shell (~ 1 -mm scale length). Interaction of the short-pulse laser with the cone generates hot electrons that accelerate surface contaminant protons from the ablated plasma.

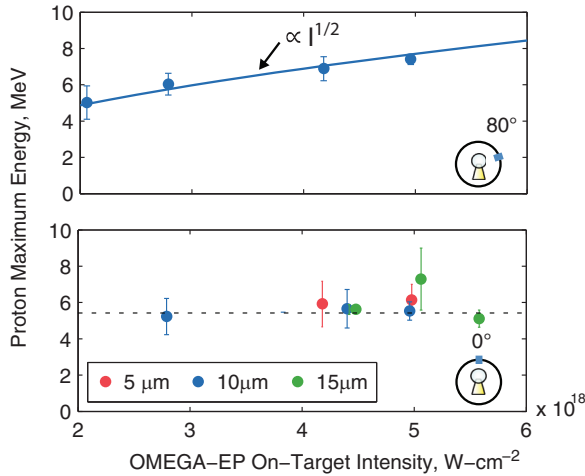


FIG. 4. Maximum proton energies measured by WRF spectrometers at 80° and 0° (where 0° corresponds to the forward short-pulse beam direction). The data points shown are averages over many WRF measurements at one location. The error bars were computed from the standard deviation of these multiple measurements. At 80° , the data show reasonable agreement with the ponderomotive hot-electron scaling. The max. proton energies for the forward beam direction (0°) neither show scaling with intensity nor dependence on cone-tip thickness.

scale with intensity as expected from theory, these protons can also be used together with models to estimate a hot-electron temperature, albeit with some caveats (see Sec. V).

In contrast to the transverse direction, the maximum energies of forward going protons (0°) neither show such scaling nor a dependence on cone-tip thickness. In addition, the maximum energies of forward-going protons are lower compared to the transverse going protons. This is consistent with simulations,²² which indicate that for these experiments, the angular distribution of hot electrons is azimuthally symmetric and has a maximum at 57° relative to the forward short-pulse beam direction and falls off at lower and higher angles. As a result, it is expected that fewer and less energetic protons would be observed in the forward direction even when the cone tip is intact, which is consistent with these measurements.

Forward-going protons are accelerated from the surfaces of the compressed shell or the surrounding blowoff plasma by hot electrons that have interacted with the compressed core and lost a significant amount of energy (Fig. 3). Some of the slower electrons are even ranged out in the core. The electron temperatures and previously measured ρR of the compressed shell ($\sim 150\text{ mg}\text{-cm}^{-2}$) are consistent with this notion, as discussed further in Sec. V. As a result, the velocity distribution of forward-going electrons has a lower maximum energy and empty regions in velocity-space, thereby reducing the energies of forward-going protons relative to transverse protons.

Several WRFs were used to obtain the average maximum proton energies at each location. The standard deviations of these measurements were used to compute the error bars shown in Fig. 4. Since the spatial separation between adjacent WRFs is of order several centimeters, the observed uncertainties in the data arise from the absolute measurement uncertainty of each WRF ($\pm 200\text{--}300\text{ keV}$) and possible spa-

tial variations in the maximum energy of the emitted protons. For the case of forward-going protons, the uncertainties are as large as $\pm 2\text{ MeV}$, which is larger than the absolute measurement uncertainty of the WRF spectrometers. Thus, we conclude that there are real spatial variations of the maximum proton energy for forward-going protons. These observed larger spatial variations could be the reason why the scaling with intensity is not readily apparent. Furthermore, these variations are consistent with (though not an indicator of) the presence of a stochastic process, such as electrons scattering in the compressed shell. For these reasons, it is difficult to estimate a hot-electron temperature from forward-going protons, as additional physics about the electron transport must be unfolded. We defer to only transverse-going protons when estimating hot-electron temperatures in Sec. V.

IV. SOURCE OF THE PROTONS

There is evidence that the observed protons are accelerated from the entire cone surface rather than the tip alone. The data presented throughout this paper were primarily obtained with 1.2-mm-long cones, with 10- μm or 40- μm tip diameters and variable tip thickness. On a few shots, cones with a length of 1.8 mm were also irradiated. Full spectral measurements of the fast protons were not available for the 1.8-mm-long cones, but the maximum proton energies for these cones were almost twice as high ($\sim 8\text{--}9\text{ MeV}$) as those of the 1.2-mm-long cones under the same laser conditions. In contrast, differences in the maximum proton energies were not observed between cones with 10- μm and 40- μm tip diameters (lengths of 1.2 mm). The cone length thus has an effect on proton acceleration, while the cone tip diameter does not.

The effect of the cone length on proton acceleration was also observed in the yield of (p,n) reactions, which come from fast protons reacting with the aluminum target chamber. The resulting neutron time-of-flight (nTOF)²³ data are shown in Fig. 5. For these two shots the nTOF settings, laser drive and target parameters were identical with the exception of the cone length. The x-ray flash, which comes from the short-pulse beam hitting the cone, and the 2.45-MeV DD-neutron signals are characteristic of these implosions. In between these signals (shown in Fig. 5), there exist a number of smaller peaks associated with neutrons from (p,n) reactions. The occurrence of the first (p,n) events are consistent with the time-of-flight of fast protons across the target chamber. The integral of these signals between the proton arrival time (e.g., $\sim 300\text{ ns}$ for 7.5 MeV protons) through 900 ns (excluding the DD-n peak) was computed for three shots: 2 with 1.2-mm-long cones 1 with a 1.8-mm-long cone. The ratio of the integrals between the 1.2- and 1.8-mm-long cone data were found to be 2.0 ± 0.5 and 3.0 ± 0.3 . These ratios are comparable to the increase in surface area of between the two cones (a factor 2.25). The cross section for (p,n) in aluminum is not available for the relevant proton energies ($< 10\text{ MeV}$), but the (p,*) cross section increases linearly from 1–5 MeV incident proton energy, and flattens out above that through 10 MeV.²⁴ The observed increase in (p,n)

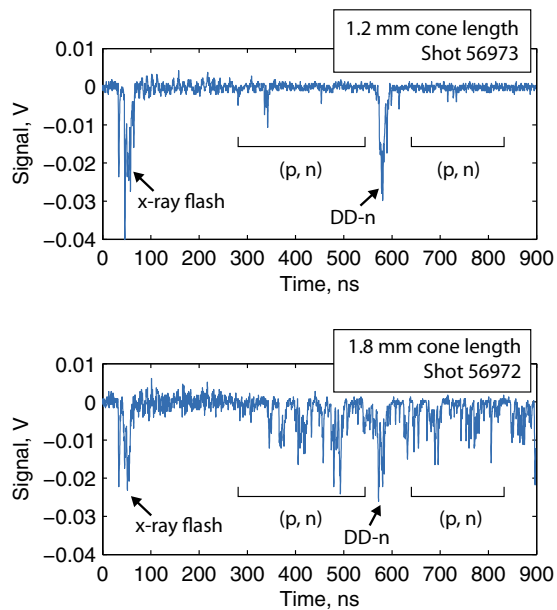


FIG. 5. Neutron time-of-flight signal, showing the x-ray flash, 2.45 MeV DD-n signal and neutrons from (p,n) reactions. For these two shots, all laser and target parameters were identical with the exception of the cone length, which was 50% greater, corresponding to 2.25 times more surface area. The ratio of the total (p,n) signal of these two cone lengths is ~ 2 –3, roughly proportional to the ratio of the cone surface areas.

reactions for 1.8 mm cones is thus attributed to a combination of higher fast-proton yields and variation of the (p,n) cross section with incident proton energy.

Throughout the course of these experiments, the timing between the long-pulse OMEGA and short-pulse OMEGA EP beams was varied to find the optimal timing of the EP beam for maximum core heating and yield. Optimal timing corresponds to core heating at peak compression of the cold dense core.¹⁵ For effective coupling of the short-pulse laser energy to the dense core, the cone tip must be intact when the short-pulse laser is fired. Shockwaves launched into the fuel during compression by the long-pulse OMEGA beams will eventually reach the cone tip, break through, and destroy it.¹⁵ In this scenario, we expect poor hot electron production and hence less energetic protons. The cone tip was intact for data shown in Fig. 4. For two shots, the timing between OMEGA and OMEGA EP was such that the tip was broken by the shockwaves when the short-pulse laser arrived at the tip. Shown in Fig. 6 are data taken at 80° using CPS1, alongside with data from WRFs (80°). The CPS1 data are generally in excellent agreement with the WRF data. This is expected since these instruments are at the same polar angle. The two shots where the tip was broken are indicated by the open circles. The maximum proton energies were significantly lower ($\sim 40\%$) when the tip was not intact.

The drastic effect of the cone tip's destruction on electron production and subsequent proton acceleration was not observed in the forward-direction, as shown in Fig. 7. For two shots, the $10\text{-}\mu\text{m}$ -thick cone tip was shocked before the short-pulse laser arrived at the cone tip. The previously measured shock break-out time,¹⁵ which varies with tip thickness is indicated in Fig. 7. Thus, neither the presence

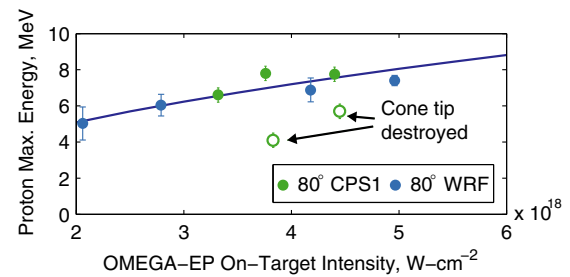


FIG. 6. Maximum proton energies measured by CPS1 and WRFs. The different CPS1 and WRF measurements (at 80°) show good agreement with one another, despite the fact that they sample different azimuthal angles. The solid line is a fit to the data ($\propto I^{1/2}$), the max. energies of the transverse protons depend on whether the cone tip is intact when the OMEGA EP short-pulse laser arrives at the tip. When not intact (open circles), the maximum energy of the transverse protons (and hence the fields that accelerate them) are lower.

of the cone tip nor the thickness of the tip (per Fig. 4) affects the acceleration of protons emitted in the forward direction.

V. ESTIMATES OF HOT-ELECTRON TEMPERATURE

It has been suggested that the presence of a significant preformed plasma inside the cone can lead to filamentation and self-focusing of the short-pulse laser, leading to higher hot-electron temperatures.^{15,25} In particular, simulations for these experiments suggest that a preformed plasma with a scale length of $100\ \mu\text{m}$ is present within the cone at the arrival time of the short-pulse OMEGA EP laser.¹⁵ The large preformed plasma, if present, is due to the laser prepulse that arises from amplified spontaneous emission (ASE). The prepulse is characterized by the laser contrast, defined as the amplitude ratio of the main drive to the prepulse. For these experiments, the energy and power contrast were 10^4 and 10^6 , respectively.¹⁵

Hotter electron temperatures, due either to self-focusing or to another physical mechanism, result in more energetic electrons that would not stop in the core as intended, thereby lowering the overall CE. Using the proton data presented in this work, we can place a lower bound on the initial hot-electron temperature to see whether the electrons are hotter than expected from the ponderomotive scaling.

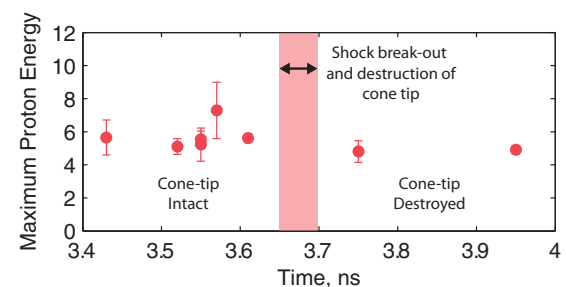


FIG. 7. Maximum energies of forward-going protons as a function of the OMEGA EP arrival time at the cone tip relative to the start of the long-pulse drive. Forward-going protons show no significant dependence on whether the cone tip is intact when the OMEGA EP short-pulse laser arrives at the cone tip. The shock breakout time at the cone tip, which depends on cone-tip thickness, occurs between 3.65 ns and 3.7 ns, as indicated.

The hot-electron temperature is estimated using a plasma expansion model, which links the temperature of an initial hot-electron distribution to the proton maximum energies. In particular, $E_M = \alpha T_H$,²¹ where α depends on the expansion model.^{8–10,26} In general, α has a logarithmic dependence on the hot-electron density (n_0) and the laser pulse duration. The choice of appropriate model depends only on the relative timescales of the laser pulse duration (τ_l) and the transit time of electrons through the cone wall (τ_e).⁹ For these experiments, $\tau_l \sim 20\tau_e$. Thus, during the first part of the laser pulse, the cone tip is completely populated with hot electrons generated from the preformed plasma on the inside of the cone. For the remainder of the pulse duration, the laser maintains the temperature of these electrons. After the pulse turns off, the electrons expand adiabatically, giving their energy to the ions. A 1D fluid model has been previously used to describe this process. This two-phase fluid model^{9,26} treats the laser as a source term that acts to maintain a steady temperature during the pulse (isothermal expansion), and then conserves energy between electrons, ions and the accelerating field thereafter (adiabatic expansion).

The two-phase model relates the hot-electron temperature to the maximum proton energy by the relation:

$$T_H = E_M \times [2.5 + 0.92 \ln(\omega_{pi} \tau_l)]^{-1}, \quad (1)$$

where T_H , E_M , ω_{pi} , and τ_l are the hot-electron temperature, max. proton energy, ion plasma frequency ($\omega_{pi} \equiv [n_{e0}e^2/m_p\epsilon_0]^{1/2}$) and the laser pulse duration, respectively. This formula was interpolated from numerical simulations²⁶ and applies for $\omega_{pi} \tau_l$ in the range of 5–100. The maximum energies and laser pulse duration were measured for each shot, while n_{e0} and hence ω_{pi} were estimated using a variation of a known method.¹¹ First, we determined the number of hot electrons generated by the short-pulse laser. Recent experiments on OMEGA EP showed that the laser energy conversion efficiency to hot electrons is 20% for such kilojoule-class short-pulse lasers,¹⁹ and that it is independent of the laser intensity. The number of hot electrons (N_e) is then found by dividing the laser energy converted to hot electrons by the average energy of the electrons, defined by the hot-electron temperature. For the experiments presented in this work, we estimate (self-consistently, from the results of this calculation) that N_e is about 10^{14} – 10^{15} . Next we obtained the volume by taking the product of the surface area of the cone and the characteristic scale length along the expansion dimension, given by $\approx c \times \tau_l$. The hot-electron density is then just the ratio of the number of hot electrons to volume. Since the plasma frequency ultimately depends on the hot-electron temperature through the density, Eq. (1) is transcendental and must be solved numerically.

It is important to recognize that the density computed here ($n_{e0} \sim 10^{17} \text{ cm}^{-3}$) is an overestimate. As discussed in Sec. IV, the protons are predominantly accelerated from either the surfaces of the cone or within the blowoff plasma surrounding it. In this calculation, we assumed that the hot-electron density is uniform, which is generally not the case. We expect the hot-electron densities to be lower upstream of the cone tip, where the ions are accelerated. From Eq. (1), it

is evident that for a given maximum proton energy, an upper bound on n_{e0} , and hence on ω_{pi} , corresponds to a lower-limit on the estimated hot-electron temperature.

Even though these ion expansion models primarily apply to thin-foil experiments,^{11,12} they can be used in the context of this work. However, a major distinction between thin-foil experiments and those presented here must be considered to allow for a correct interpretation of the data taken in this work. The scale length of the ion front where the protons are accelerated is very different in these experiments. The two-phase model used here assumes that the initial scale length of this front is small in comparison to the hot-electron Debye length. While this is true for typical thin-foil experiments with short-pulse lasers, in our case the scale length of the blowoff plasma in front of the cone is $\sim 400 \mu\text{m}$ –1 mm due to the implosion of the shell. The effective scale length seen by the accelerating protons is roughly of this order, whereas the hot-electron Debye length is $\sim 20 \mu\text{m}$. In this case, the maximum proton energies are lower since they scale inversely with the initial density scale length at the ion front.²⁷ To quantify this difference to some extent, it has been shown that the addition of a 100- μm -scale-length plasma at the ion expansion front (in a scale length otherwise dominated by the much smaller hot-electron Debye length), reduced the observed maximum proton energies by about 4 times.²⁷ Thus, for a given hot-electron temperature, the proton energies from these experiments are much smaller than expected by the model because of the longer scale length. Hence, in applying the expansion model to these experiments, it is expected that the actual temperatures are much higher than the temperatures estimated using the model. While this may seem uncertain, the aim is not to pinpoint the exact temperature, but to show that it is significantly hotter than expected from the ponderomotive scaling.

We used protons at 80° to estimate the hot-electron temperature, as these protons demonstrated the expected scaling with intensity ($\propto I^{1/2}$). For each shot, Eq. (1) was solved numerically to determine the lower-limit of the hot-electron temperature, and the results are shown in Fig. 8. The error bars correspond to the uncertainty of the maximum proton energy measurement. Shown alongside these data is the ponderomotive vacuum scaling (for the case of negligible pre-plasma inside the cone). The temperatures determined

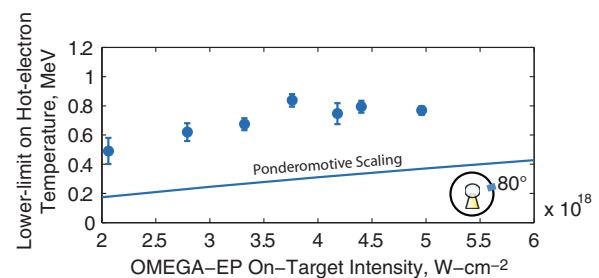


FIG. 8. Lower-limit on the initial hot-electron temperatures as a function of the incident short-pulse laser intensity. These temperatures were determined using the maximum proton energies 80° together with ion expansion models. Shown alongside the data is the ponderomotive prediction of the hot-electron temperature for the case of negligible preformed plasma inside the cone. These temperatures are factors of 2–3 higher than expected.

here are factors of 2–3 higher than the vacuum scaling. If this increase in temperature is due entirely to laser self-focusing in the pre-plasma, this result corresponds to a factor of 3–10 enhancement of the incident laser intensity.

It is worth noting that OMEGA EP is known to produce maximum proton energies that are higher in comparison to those of other laser systems.²⁸ In particular, it has been shown that for a fixed laser intensity ($\sim 2\text{--}8 \times 10^{18} \text{ W}\cdot\text{cm}^{-2}$), the maximum proton energy increases as the pulse duration is increased from 1 ps to 10 ps.²⁹ Observations indicate that the maximum proton energy on OMEGA EP increases faster with the laser pulse duration than models (for example, Eq. (1)) predict. At present, there is no explanation for this observation. We speculate that the effect itself could be due to hotter electron temperatures (for instance, due to enhanced absorption or to hot-electron refluxing) for longer pulses (10 ps), or due to additional physics of the ion acceleration process that is not incorporated into the models at this point.

Finally, these temperatures are consistent with the notion that many of the hot electrons that are emitted at 0° can penetrate, escape the compressed shell and accelerate surface ions in the forward direction as shown in Sec. III. The average ρR of the compressed shell for spherical implosions with comparable laser and target parameters has been previously measured to be about $\sim 150 \text{ mg}\cdot\text{cm}^{-2}$.¹⁵ Given this dense core, electrons generated on one side near the cone tip, would need energies of $\geq 500 \text{ keV}$ to penetrate and escape the core, a condition that is readily satisfied by the temperatures shown in Fig. 8.

VI. CONCLUSION

In this work, we have for the first time characterized the energy loss to fast protons in cone-in-shell fast-ignitor experiments. We estimate that of order 10 J, or 1% of the short-pulse laser energy is lost to fast protons. It was shown that these protons are accelerated from the surface of the cone, rather than the cone tip alone.

Finally, we have used these protons to estimate a lower bound on the initial hot-electron temperature. These estimated hot-electron temperatures (500–900 keV) are hotter than predicted from the ponderomotive scaling by factors of 2–3. If the enhancement of the hot-electron temperature is due entirely to laser self-focusing, this result corresponds to a factor of 3–10 enhancement of the incident laser intensity.

ACKNOWLEDGMENTS

This work was supported in part by the Fusion Science Center (Rochester Sub Award PO No. 415023-G), National Laser User's Facility (DOE Award No. DE-NA0000877), US DOE (Grant No. DE-FG52-09NA29553), Laboratory for Laser Energetics (LLE) (No. 414090-G), and Lawrence Livermore National Laboratory (No. B580243).

¹N. G. Basov, S. Yu. Gus'kov, and L. P. Feokistov, "Thermonuclear gain of ICF targets with direct heating of ignitor," *J. Russ. Laser Res.* **13**, 396–399 (1992).

²M. Tabak, J. Hammer, M. E. Glinsky, W. L. Kruer, S. C. Wilks, J. Woodworth, E. Michael Campbell, M. D. Perry, and R. J. Mason, "Ignition and

high gain with ultrapowerful lasers," *Phys. Plasmas* **1**(5), 1626–1634 (1994).

³D. G. Hicks, C. K. Li, F. H. Séguin, J. D. Schnittman, A. K. Ram, J. A. Frenje, R. D. Petrasso, J. M. Soares, D. D. Meyerhofer, S. Roberts, C. Sorce, C. Stockl, T. C. Sangster, and T. W. Phillips, "Observations of fast protons above 1 MeV produced in direct-drive laser-fusion experiments," *Phys. Plasmas* **8**(2), 606–610 (2001).

⁴A. B. Zylstra, C. K. Li, F. H. Séguin, M. J. Rosenberg, H. G. Rinderknecht, N. Sinenian, J. A. Frenje, R. D. Petrasso, N. Izumi, P. A. Amendt, O. L. Landen, and J. A. Koch, "Measurements of hohlraum-produced fast ions," *Phys. Plasmas* **19**(4), 042707 (2012).

⁵P. McKenna, F. Lindau, O. Lundh, D. Neely, A. Persson, and C.-G. Wahlstrom, "High-intensity laser-driven proton acceleration: influence of pulse contrast," *Philos. Trans. R. Soc. London, Ser. A* **364**(1840), 711–723 (2006).

⁶S. S. Bulanov, A. Brantov, V. Yu. Bychenkov, V. Chvykov, G. Kalinchenko, T. Matsuoka, P. Rousseau, S. Reed, V. Yanovsky, D. W. Litzenberg, K. Krushelnick, and A. Maksimchuk, "Accelerating monoenergetic protons from ultrathin foils by flat-top laser pulses in the directed-coulomb-explosion regime," *Phys. Rev. E* **78**, 026412 (2008).

⁷K. A. Flippo, E. d'Humieres, S. A. Gaillard, J. Rassuchine, D. C. Gautier, M. Schollmeier, F. Numberg, J. L. Kline, J. Adams, B. Albright, M. Bakenman, K. Harres, R. P. Johnson, G. Korgan, S. Letzring, S. Malekos, N. Renard-LeGalloudec, Y. Sentoku, T. Shimada, M. Roth, T. E. Cowan, J. C. Fernandez, and B. M. Hegelich, "Increased efficiency of short-pulse laser-generated proton beams from novel flat-top cone targets," *Phys. Plasmas* **15**(5), 056709–12 (2008).

⁸P. Mora, "Plasma expansion into a vacuum," *Phys. Rev. Lett.* **90**(18), 185002 (2003).

⁹P. Mora, "Thin-foil expansion into a vacuum," *Phys. Rev. E* **72**, 056401 (2005).

¹⁰P. Mora, "Collisionless expansion of a gaussian plasma into a vacuum," *Phys. Plasmas* **12**(11), 112102 (2005).

¹¹J. Fuchs, P. Antici, E. d'Humieres, E. Lefebvre, M. Borghesi, E. Brambrink, C. A. Cecchetti, M. Kaluza, V. Malka, M. Manclossi, S. Meyroneinc, P. Mora, J. Schreiber, T. Toncian, H. Pepin, and P. Audebert, "Laser-driven proton scaling laws and new paths towards energy increase," *Nat. Phys.* **2**(1), 48–54 (2006).

¹²L. Robson, P. T. Simpson, R. J. Clarke, K. W. D. Ledingham, F. Lindau, O. Lundh, T. McCanny, P. Mora, D. Neely, C. G. Wahlstrom, M. Zepf, and P. McKenna, "Scaling of proton acceleration driven by petawatt-laser-plasma interactions," *Nat. Phys.* **3**(1), 58–62 (2007).

¹³T. R. Boehly, D. L. Brown, R. S. Craxton, R. L. Keck, J. P. Knauer, J. H. Kelly, T. J. Kessler, S. A. Kumpan, S. J. Loucks, S. A. Letzring, F. J. Marshall, R. L. McCrory, S. F. B. Morse, W. Seka, J. M. Soares, and C. P. Verdon, "Initial performance results of the OMEGA laser system," *Opt. Commun.* **133**(1–6), 495–506 (1997).

¹⁴L. J. Waxer, D. N. Maywar, J. H. Kelly, T. J. Kessler, B. E. Kruschwitz, S. J. Loucks, R. L. McCrory, D. D. Meyerhofer, S. F. B. Morse, C. Stockl, and J. D. Zuegel, "High-energy petawatt capability for the OMEGA laser," *Opt. Photonics News* **16**(7), 30–36 (2005).

¹⁵W. Theobald, A. A. Solodov, C. Stockl, K. S. Anderson, R. Betti, T. R. Boehly, R. S. Craxton, J. A. Delettrez, C. Dorrer, J. A. Frenje, V. Yu. Glebov, H. Habara, K. A. Tanaka, J. P. Knauer, R. Lauck, F. J. Marshall, K. L. Marshall, D. D. Meyerhofer, P. M. Nilson, P. K. Patel, H. Chen, T. C. Sangster, W. Seka, N. Sinenian, T. Ma, F. N. Beg, E. Giraldez, and R. B. Stephens, "Initial cone-in-shell fast-ignition experiments on OMEGA," *Phys. Plasmas* **18**(5), 056305 (2011).

¹⁶F. H. Séguin, J. A. Frenje, C. K. Li, D. G. Hicks, S. Kurebayashi, J. R. Rygg, B. E. Schwartz, R. D. Petrasso, S. Roberts, J. M. Soares, D. D. Meyerhofer, T. C. Sangster, J. P. Knauer, C. Sorce, V. Yu. Glebov, C. Stockl, T. W. Phillips, R. J. Leeper, K. Fletcher, and S. Padalino, "Spectrometry of charged particles from inertial-confinement-fusion plasmas," *Rev. Sci. Instrum.* **74**(2), 975–995 (2003).

¹⁷N. Sinenian, M. J. Rosenberg, M. Manuel, S. C. McDuffee, D. T. Casey, A. B. Zylstra, H. G. Rinderknecht, M. Gatu Johnson, F. H. Séguin, J. A. Frenje, C. K. Li, and R. D. Petrasso, "The response of CR-39 nuclear track detector to 1–9 MeV protons," *Rev. Sci. Instrum.* **82**(10), 103303 (2011).

¹⁸D. G. Hicks, C. K. Li, F. H. Séguin, A. K. Ram, J. A. Frenje, R. D. Petrasso, J. M. Soares, V. Yu. Glebov, D. D. Meyerhofer, S. Roberts, C. Sorce, C. Stockl, T. C. Sangster, and T. W. Phillips, "Charged-particle acceleration and energy loss in laser-produced plasmas," *Phys. Plasmas* **7**(12), 5106–5117 (2000).

- ¹⁹P. M. Nilson, A. A. Solodov, J. F. Myatt, W. Theobald, P. A. Jaanimagi, L. Gao, C. Stoeckl, R. S. Craxton, J. A. Delettrez, B. Yaakobi, J. D. Zuegel, B. E. Kruschwitz, C. Dorrer, J. H. Kelly, K. U. Akli, P. K. Patel, A. J. Mackinnon, R. Betti, T. C. Sangster, and D. D. Meyerhofer, "Scaling hot-electron generation to high-power, kilojoule-class laser-solid interactions," *Phys. Rev. Lett.* **105**, 235001 (2010).
- ²⁰S. P. Hatchett, C. G. Brown, T. E. Cowan, E. A. Henry, J. S. Johnson, M. H. Key, J. A. Koch, A. Bruce Langdon, B. F. Lasinski, R. W. Lee, A. J. Mackinnon, D. M. Pennington, M. D. Perry, T. W. Phillips, M. Roth, T. Craig Sangster, M. S. Singh, R. A. Snavely, M. A. Stoyer, S. C. Wilks, and K. Yasuike, "Electron, photon, and ion beams from the relativistic interaction of petawatt laser pulses with solid targets," *Phys. Plasmas* **7**(5), 2076–2082 (2000).
- ²¹S. C. Wilks, A. B. Langdon, T. E. Cowan, M. Roth, M. Singh, S. Hatchett, M. H. Key, D. Pennington, A. MacKinnon, and R. A. Snavely, "Energetic proton generation in ultra-intense laser-solid interactions," *Phys. Plasmas* **8**(2), 542–549 (2001).
- ²²J. Li, J. R. Davies, C. Ren, A. Solodov, W. Theobald, J. Tonge, and W. B. Mori, "Hot electron generation from laser-cone target interactions in fast ignition," *Bull. Am. Phys. Soc.* **53**, 222 (2011).
- ²³C. Stoeckl, M. Cruz, V. Yu. Glebov, J. P. Knauer, R. Lauck, K. Marshall, C. Mileham, T. C. Sangster, and W. Theobald, "A gated liquid-scintillator-based neutron detector for fast-ignitor experiments and down-scattered neutron measurements," *Rev. Sci. Instrum.* **81**(10), 10D302 (2010).
- ²⁴See <http://www.nndc.bnl.gov/> for ENDF/B-VII.0 Library.
- ²⁵A. A. Solodov, K. S. Anderson, R. Betti, V. Gotcheva, J. Myatt, J. A. Delettrez, S. Skupsky, W. Theobald, and C. Stoeckl, "Integrated simulations of implosion, electron transport, and heating for direct-drive fast-ignition targets," *Phys. Plasmas* **16**(5), 056309 (2009).
- ²⁶P. Mora, "Laser driven ion acceleration," *AIP Conf. Proc.* **920**(1), 98–117 (2007).
- ²⁷A. J. Mackinnon, M. Borghesi, S. Hatchett, M. H. Key, P. K. Patel, H. Campbell, A. Schiavi, R. Snavely, S. C. Wilks, and O. Willi, "Effect of plasma scale length on multi-MeV proton production by intense laser pulses," *Phys. Rev. Lett.* **86**, 1769–1772 (2001).
- ²⁸K. Flippo, T. Bartal, F. Beg, S. Chawla, J. Cobble, S. Gaillard, D. Hey, A. MacKinnon, A. MacPhee, P. Nilson, D. Offermann, S. Le Pape, and M. J. Schmitt, "Omega EP, laser scalings and the 60 MeV barrier: First observations of ion acceleration performance in the 10 picosecond kilojoule short-pulse regime," *J. Phys.: Conf. Ser.* **244**(2), 022033 (2010).
- ²⁹L. Gao, P. M. Nilson, W. Theobald, C. Stoeckl, C. Dorrer, T. C. Sangster, D. D. Meyerhofer, L. Willingale, and K. M. Krushelnick, "Measurements of proton generation with intense, kilojoule laser pulses on OMEGA EP," *Bull. Am. Phys. Soc.* **55**(15) (2010).